Technical note: Nonrigid registration for laparoscopic liver surgery using sparse intraoperative data

Jon S. Heiselman[1,2], Jarrod A. Collins[1,2], Logan W. Clements[1,2], Jared A. Weis[3], Amber L. Simpson[4], Sunil K. Geevarghese[5], T. Peter Kingham[4], William R. Jarnagin[4], and Michael I. Miga[1,2,6,7]

[1]Department of Biomedical Engineering, Vanderbilt University, Nashville, TN, USA
[2]Vanderbilt Institute in Surgery and Engineering, Vanderbilt University, Nashville, TN, USA
[3]Department of Biomedical Engineering, Wake Forest School of Medicine, Winston-Salem, NC, USA
[4]Department of Surgery, Memorial Sloan-Kettering Cancer Center, New York, NY, USA
[5]Division of Hepatobiliary Surgery and Liver Transplantation, Vanderbilt University Medical Center, Nashville, TN, USA
[6]Department of Radiology and Radiological Sciences, Vanderbilt University Medical Center, Nashville, TN, USA
[7]Department of Neurological Surgery, Vanderbilt University Medical Center, Nashville, TN, USA

ABSTRACT

Soft tissue deformation can be a major source of error for image-guided interventions. Deformations associated with laparoscopic liver surgery can be substantially different from those concomitant with open approaches due to intraoperative practices such as abdominal insufflation and variable degrees of mobilization from the supporting ligaments of the liver. This technical note outlines recent contributions towards nonrigid registration for laparoscopic liver surgery published in the *Journal of Medical Imaging* special issue on image-guided procedures, robotic interventions, and modeling [10]. In particular, we review (1) a characterization of intraoperative liver deformation from clinically-acquired sparse digitizations of the organ surface through a series of laparoscopic-to-open conversions, and (2) a novel deformation correction strategy that leverages a set of control points placed across anatomical regions of mechanical support provided to the organ. Perturbations of these control points on a finite element model were used to iteratively reconstruct the intraoperative deformed organ shape from sparse measurements of the liver surface. These characterization and correction methods for laparoscopic deformation were applied to a retrospective clinical series of 25 laparoscopic-to-open conversions performed under image guidance and a phantom validation framework.

Keywords: Laparoscopy, image-guided surgery, registration, soft tissue deformation, liver, finite element model

1. INTRODUCTION

In liver interventions such as resection and ablation, reliable localization of subsurface structures is required to guide resection planes and accurately deliver treatment. While manual palpation is conventional for identifying these structures during open procedures, this technique is not typically available during laparoscopy. As a result, laparoscopic interventions are often restricted by the ability of the surgeon to approximate the intraoperative positions of lesions and vessels from unregistered preoperative image volumes or experiential knowledge. Simultaneously, approximately 10% of all major laparoscopic resections are converted to open procedures [1]. Principally, intraoperative events that lead to conversion include excessive bleeding, unintended damage to peripheral structures, and concerns over oncological margins [2]. During laparoscopy, the restricted ability to maneuver tools and intraoperatively locate internal structures of the liver may encumber parenchymal transection and contribute to the frequently reported steep learning curve of laparoscopic liver resection [3–5]. With successful laparoscopic approaches providing significant short-term benefits to patients such as significantly faster recovery, fewer postoperative complications, and similar oncological adequacy [6–7], the high rate of conversion likely signals limitations in current laparoscopic guidance technology.

Image guidance may be able to assist the delivery of laparoscopic interventions through registration of rich feature information from high quality preoperative image volumes to the patient. However, laparoscopic image guidance is typically challenged by considerable deformation existing between the preoperative and intraoperative organ shapes. Insufflation, a process where the abdominal cavity is pressurized with carbon dioxide, causes expansion of the abdominal cavity and likely is a major source of liver deformation. Porcine models of abdominal insufflation demonstrate that vessel centerlines can shift up to 35 mm and experience nonrigid deformations of more than 11 mm [8]. Anatomically, insufflation causes distension of the abdominal wall and diaphragm [9], which are joined to the liver by the falciform and triangular ligaments, respectively. Upon insufflation, these ligaments may conduct forces from abdominal motions and influence the shape of the liver. Additionally, insufflation may displace the bowel and other structures that normally provide mechanical support on the posterior surface of the liver. Intraoperative laparoscopic deformations are further accentuated by mobilization of the liver from its supporting ligaments, which may be done to varying degrees of completion.

In a recent contribution to the *Journal of Medical Imaging* [10], we reported (1) a method for measuring the laparoscopic deformations from a clinical data series obtained during laparosopic image guidance, and (2) a nonrigid registration strategy for intraoperatively correcting laparoscopic deformation and producing an accurate mapping between preoperative and intraoperative organ configurations. In this technical note, we review the progress made towards both aims of this work.

2. CHARACTERIZATION OF LAPAROSCOPIC DEFORMATION

No other studies have been performed in a clinical setting to characterize the magnitude of laparoscopic liver deformation in the context of abdominal insufflation. In [10], we investigated an approach for comparing organ deformation at varying levels of insufflation. With an optically tracked stylus, sparse digitization data of the organ surface were collected at three intraoperative stages throughout the course of 25 clinical cases of laparoscopic-to-open conversion. Laparoscopic surface collections were obtained first at standard insufflation pressure of 14 mmHg, then at reduced insufflation pressure of 7 mmHg. A third organ surface digitization was obtained for each patient after conversion to open approach. The study consisted of a pairwise, paired analysis of the relative magnitudes of deformation between the shapes of the liver during (a) preoperative imaging, (b) laparoscopic approach at standard insufflation pressure and (c) reduced insufflation pressure, and (d) during open surgery. Briefly, as shown in Figure 1, pairs of sparse surface data collections corresponding to different intraoperative deformations of each liver were rigidly registered to a liver model segmented from preoperative images. Uniformly sampled surface reconstructions were generated from these surface data using a previously characterized resampling strategy [11]. Within the overlapping regions of reconstructed surface pairs, the average surface dissimilarity was computed using the modified Hausdorff distance (MHD) as a metric for evaluating the severity of deformation existing between organ configurations.

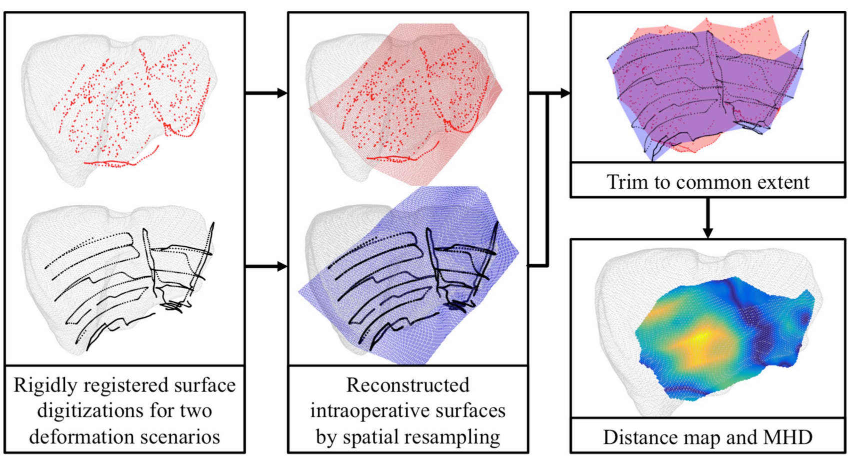

Figure 1. Procedure for assessing deformation between sparse digitizations of organ surfaces. Reproduced from [10].

Table 1 summarizes the results from our characterization study of laparoscopic deformation. We found that all pairwise MHD distributions were significantly greater than zero, indicating that substantial deformation occurred between every pair of organ configurations examined, from the preoperative presentation through insufflation and laparoscopic-to-open conversion. Importantly, simply reducing insufflation pressure from 14 mmHg to 7 mmHg produced a significant change in liver shape. These results show that the intraoperative shape of the liver is sensitive to insufflation pressure and that standard insufflation produces deformations of approximately 10 mm on average across the observed organ surface.

	Preop	**Lap14mmHg**	**Lap7mmHg**	**Open**
Preop	0	10.1 ± 5.9	9.0 ± 7.0	7.4 ± 4.6
Lap14mmHg		0	6.4 ± 2.6	6.6 ± 3.3
Lap7mmHg			0	6.3 ± 2.5
Open				0

Table 1. Modified Hausdorff distance (mean ± std) in mm between pairs of preoperative (Preop), laparoscopic (Lap14mmHg, Lap7mmHg) and open (Open) liver configurations for n=25 clinical cases. Reproduced from [10].

Paired comparative analysis of the MHD showed that deformations related to the initial transitions from preoperative to laparoscopic organ configurations at standard insufflation were significantly larger than subsequent deformations associated with reducing insufflation pressure or converting to open (first diagonal in Table 1). Also, compared to the preoperative organ shape, deformations under standard laparoscopic insufflation pressure were significantly larger than deformations associated with the open approach (top row in Table 1). The large deformations that occur between preoperative assessment and laparoscopic intervention at standard insufflation pressure suggest that accounting for deformation in laparoscopic image-to-physical registrations is likely to be very important.

3. CORRECTION OF LAPAROSCOPIC DEFORMATION

In addition to characterizing the degree of laparoscopic deformation, the second aim of [10] was to introduce a nonrigid registration method based on the anatomical constraints imparted by the laparoscopic surgical approach and to perform a quantitative feasibility study in a phantom setup that reproduces laparoscopic liver deformation. Previously, a custom laparoscopic simulator was designed to reproduce deformation in a silicone liver phantom by suspending the liver in a mock abdominal cavity at insufflated dimensions by the three supporting anterosuperior ligaments [12]. As discussed above, forces from insufflation can be conducted to the liver through the falciform and triangular ligaments as well as through displacement of the bowel. Figure 2a shows the anatomical positions of the supporting anterosuperior ligaments and Figure 2b shows the liver phantom inside the laparoscopic simulator. The liver phantom was shaped from a 3D printed segmentation of a clinical preoperative CT scan. A total of 147 radiopaque targets were distributed throughout the volume of the phantom as demonstrated in Figure 2c to allow validation of target registration error (TRE) through subsequent CT imaging.

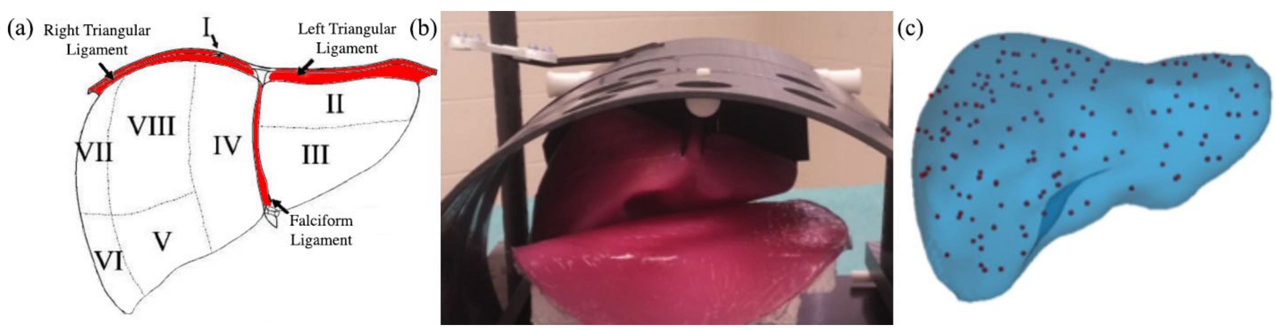

Figure 2. (a) The anterosuperior ligaments of the liver include the falciform and the left and right triangular ligaments, adapted from Kingham et al. [13] (b) The liver phantom is suspended in the mock insufflated abdomen without mobilization. (c) The validation targets are evenly dispersed throughout the phantom. Reproduced from [10].

3.1 Nonrigid Registration Algorithm

In [10], a nonrigid image-to-physical registration method was introduced for correcting laparoscopic soft tissue deformation. This method uses only sparse surface data from the anterior surface of the liver collected with an optically tracked stylus. An inverse modeling approach is taken to intraoperatively recover the configuration of the deformed organ within anatomically permitted constraints. To model deformations of the liver, a linear elastic finite element biomechanical model was used. A mesh of the liver was derived from a preoperative image volume, and series of control points were placed on each anatomical surface of the liver that grants mechanical support to the organ. Model responses to small 1-mm perturbations of each control point in the three orthogonal Cartesian directions were precomputed and stored in an effective Jacobian solution matrix. Using the principle of superposition, the observed intraoperative organ deformation can be approximated as a linear combination of model responses to perturbations of control points placed on the anatomical support surfaces. This approach leverages a priori knowledge of anatomical constraints to restrict the possible modes with which the liver may deform. An initial alignment between the sparse intraoperative anterior surface designation and the preoperative model is made using a feature-weighted iterative closest point algorithm [14], which factors out most of the rigid body motion of the organ. The set of parameters specifying the linear combination of deformation responses to control point perturbations is then iteratively optimized simultaneously with additional rigid translational and rotational components. The objective function is chosen to minimize the residual error between the deformed model and the observed sparse surface data, along with the total strain energy of the model-predicted deformation. An overview of this procedure is shown in Figure 3 and additional details can be found in [10]. This inverse solution method that optimizes for observed deformation based on precomputed control point perturbations is unique from other modeling approaches used in current nonrigid registration methods for laparoscopic organ deformations. The primary advantage of this approach is that it avoids using intraoperative data directly as boundary conditions in the model; in this way, the method becomes more robust to noisy sources of intraoperative data. Furthermore, in contrast to a previous inverse modeling approach taken by Rucker et al. for nonrigid registrations in open liver surgery [15], our method does not make any assumptions about the functional form of boundary conditions.

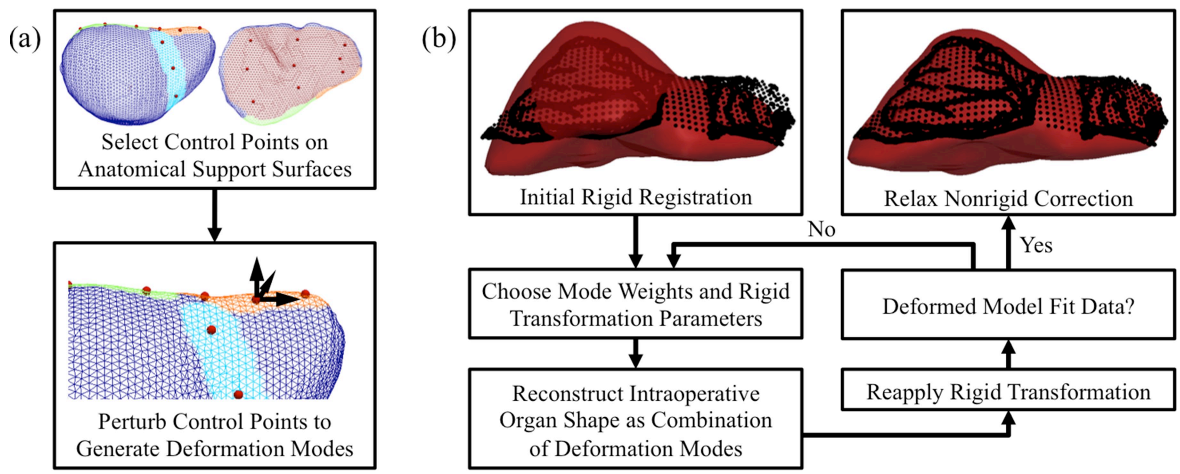

Figure 3. Overview of the nonrigid registration algorithm, reproduced from [10]. (a) A set of control points is placed on the support surfaces of the liver, including the ligament attachment regions and the posterior surface of the liver. Each control point is perturbed to generate a set of deformation modes that linearly combine to approximate the intraoperative distributed load placed across each support. (b) Starting from an initial rigid registration, a set of parameters corresponding to weights for each control point perturbation is iteratively optimized with rigid transformation parameters until the deformed model agrees with the observed surface data.

Our approach is valid because any distributed load intraoperatively applied to a support surface has a statically equivalent combination of applied control point forces. In accordance with Saint-Venant's principle, the difference between the two statically equivalent loads quickly vanishes with distance away from the support. To account for discrepancies associated with our point load approximation in the near field at the support surfaces, we perform an additional relaxation step to allow recovery of a more distributed local application of body forces at these sites.

3.2 Registration Results

Three deformations corresponding to different laparoscopic mobilization scenarios were applied to a liver phantom in the aforementioned laparoscopic simulator. We employed the previously described nonrigid registration method to correct for deformation relative to the undeformed preoperative shape of the liver phantom. Table 2 summarizes the assessment of TRE for these cases using typical extents of sparse surface data. Across cases, the nonrigid registration method reduced the average TRE to 6.37±0.47 mm, representing a 56.5% average correction over rigid registration. Figure 4a demonstrates the shift in the observed distribution of target error for a representative case. Figure 4b shows the distribution of target error after nonrigid registration within the phantom. It can be seen that target error tends to increase with distance away from intraoperative data. Furthermore, the spatial dependence of error in these results demonstrates the need for thorough sampling when evaluating target error.

Phantom Deformation	Rigid Registration (Clements et al.)	Nonrigid Registration	Correction (%)
Left Mobilization	13.16 ± 2.65	5.90 ± 4.27	55.2%
Right Mobilization	16.16 ± 6.72	7.02 ± 4.56	56.6%
No Mobilization	14.72 ± 6.53	6.20 ± 4.12	57.9%

Table 2. Target registration error (mean ± SD) in mm for simulated mobilization conditions in the phantom after rigid and nonrigid registration. Adapted from [10].

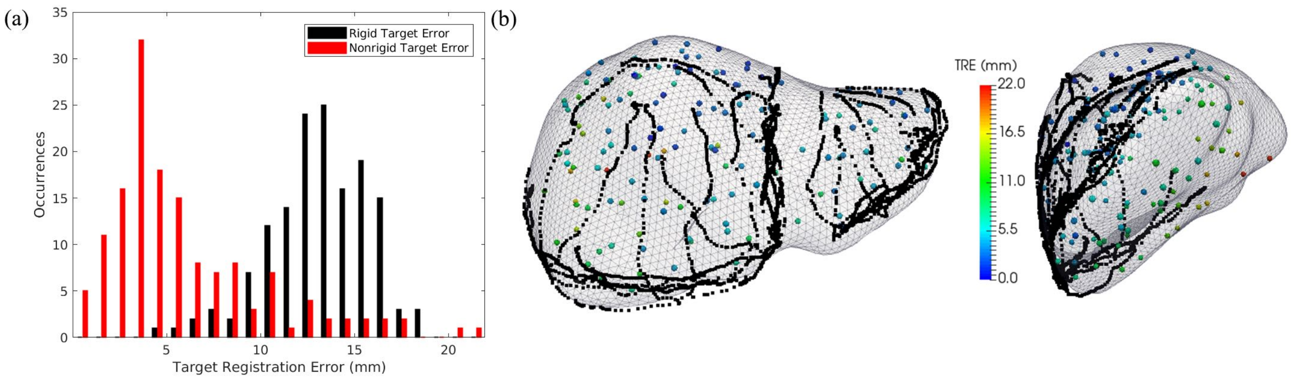

Figure 4. Target error for Left Mobilization. (a) Histogram of target registration error for rigid and nonrigid registrations. (b) Distribution of target errors after nonrigid registration throughout the phantom. Intraoperatively digitized organ surface data is shown in black.

3.3 Impact of Intraoperative Surface Data Extent

In [10], a moderate correlation was found to exist between individual target errors and the distance between the target and the closest intraoperatively digitized surface data point. Furthermore, in the clinical series of laparoscopic to open conversions, the extents of organ surface coverage were found to be highly variable; extents obtained during laparoscopic interrogation of the organ with a tracked stylus covered 22.0 ± 8.2% of the total organ surface (n=50). Interestingly, the extents of surface data obtained in the open approach were not significantly different (22.4 ± 5.4%, n=25). Nonetheless, the effects of this variability in surface data on registration accuracy were investigated. The phantom deformation study was repeated for varying extents of collected laparoscopic surface data. In our phantom framework, it was found that certain ports in the right upper quadrant provided access to larger extents of the organ surface than ports positioned laterally or in the periumbilical region. Figure 5a demonstrates the effect of surface data extent on registration accuracy. While the nonrigid registration performs poorly at low extents of surface data, at extents exceeding 22% the nonrigid registration yielded an overall average TRE of 6.7±1.3 mm across all cases. Additionally, all individual nonrigid registrations produced average TRE under 10 mm.

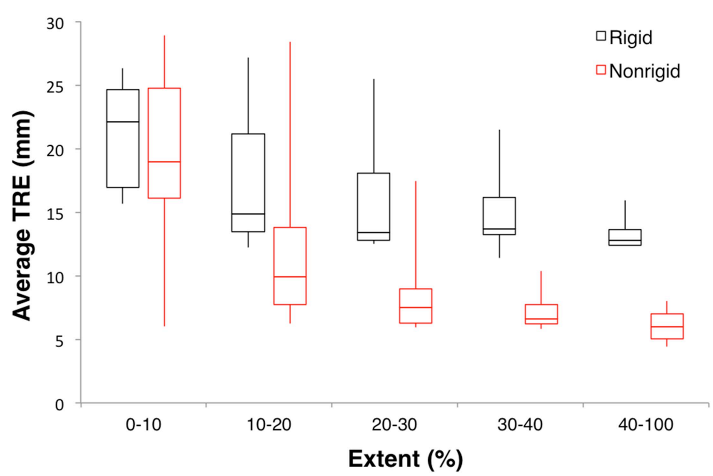

Figure 5. Quartile plot for average TRE across the liver as a function of registered intraoperative surface data extent.

Considering the clinical implications, extents exceeding 22% of the organ surface should be obtainable in most circumstances provided sufficient care is taken to acquire data with comprehensive coverage. While target errors below 5 mm would be ideal, 10 mm represents the recommended oncological margin size for liver tumors. As shown in Figure 4, regions of the liver do achieve below 5 mm of target error with our nonrigid registration. However, incomplete surface coverage can lead to inadequately constrained registrations where there is a paucity of intraoperative data.

4. CONCLUSIONS

This review of our recent work demonstrates strides towards assessing and compensating for laparoscopic deformation of the liver. While we achieve promising performance, continued work is needed to improve the accuracy of nonrigid registrations in the setting of image-guided laparoscopic liver surgery. Instrumentation methods that can improve laparoscopic access to data such as integration with laparoscopic ultrasound and more refined biomechanical models that account for effects such as ambient insufflation pressure, gravity, and material heterogeneity may be able to further advance laparoscopic image guidance for the liver.

ACKNOWLEDGEMENTS

This work was supported by the NIH-NCI grant R01CA162477 and the NIH-NIBIB training grant T32EB021937.

REFERENCES

[1] Dagher, I., Gayet, B., Tzanis, D., Tranchart, H., Fuks, D., Soubrane, O., Kim, H. H. K., Cherqui, D., Rourke, N. O., et al., "International experience for laparoscopic major liver resection," J Hepatobiliary Pancreat Sci **21**, 732–736 (2014).

[2] Halls, M. C., Cipriani, F., Berardi, G., Barkhatov, L., Lainas, P., Alzoubi, M., D'Hondt, M., Rotellar, F., Dagher, I., et al., "Conversion for Unfavorable Intraoperative Events Results in Significantly Worst Outcomes During Laparoscopic Liver Resection: Lessons Learned From a Multicenter Review of 2861 Cases," Ann. Surg. **Pre-print**, 1–7 (2017).

[3] Kluger, M. D., Vigano, L., Barroso, R., Cherqui, D., "The learning curve in laparoscopic major liver resection," J Hepatobiliary Pancreat Sci **20**(10), 131–136 (2013).

[4] Nomi, T., Fuks, D., Kawaguchi, Y., Mal, F., Nakajima, Y., Gayet, B., "Learning curve for laparoscopic major hepatectomy," BJS **102**, 796–804 (2015).

[5] Brown, K. M., Geller, D. A., "What is the Learning Curve for Laparoscopic Major Hepatectomy?," J. Gastrointest. Surg. **20**, 1065–1071 (2016).

[6] Ciria, R., Cherqui, D., Geller, D. A., Briceno, J., Wakabayashi, G., "Comparative Short-term Benefits of Laparoscopic Liver Resection: 9000 Cases and Climbing," Ann. Surg. **263**(4), 761–777 (2016).

[7] Fretland, A. A., Dagenborg, V. J., Bjørnelv, G. M., Kazaryan, A. M., Kristiansen, R., Fagerland, M. W., Hausken, J., Tønnessen, T. I., Abildgaard, A., et al., "Laparoscopic Versus Open Resection for Colorectal Liver Metastases: The OSLO-COMET Randomized Controlled Trial," Ann. Surg. **267**(2), 199–207 (2018).

[8] Vijayan, S., Reinertsen, I., Hofstad, E. F., Rethy, A., Hernes, T. A. N., Langø, T., "Liver deformation in an animal model due to pneumoperitoneum assessed by a vessel-based deformable registration," Minim. Invasive Ther. **23**, 279–286 (2014).

[9] Malbrain, M. L. N. G., Peeters, Y., Wise, R., "The neglected role of abdominal compliance in organ-organ interactions," Crit. Care **20**(67), 1–10 (2016).

[10] Heiselman, J. S., Clements, L. W., Collins, J. A., Weis, J. A., Simpson, A. L., Geevarghese, S. K., Kingham, T. P., Jarnagin, W. R., Miga, M. I., "Characterization and correction of soft tissue deformation in laparoscopic image-guided liver surgery," J. Med. Imaging **5**(2), 1–13 (2018).

[11] Collins, J. A., Weis, J. A., Heiselman, J. S., Clements, L. W., Simpson, A. L., Jarnagin, W. R., Miga, M. I., "Improving Registration Robustness for Image-Guided Liver Surgery in a Novel Human-to-Phantom Data Framework," IEEE Trans. Med. Imaging **36**(7), 1502–1510 (2017).

[12] Heiselman, J. S., Collins, J. A., Clements, L. W., Weis, J. A., Simpson, A. L., Geevarghese, S. K., Jarnagin, W. R., Miga, M. I., "Emulation of the laparoscopic environment for image-guided liver surgery via an abdominal

phantom system with anatomical ligamenture," Proc. SPIE **10135**, 1–9 (2017).

[13] Kingham, T. P., Jayaraman, S., Clements, L. W., Scherer, M. A., Stefansic, J. D., Jarnagin, W. R., "Evolution of Image-Guided Liver Surgery: Transition from Open to Laparoscopic Procedures," J Gastrointest Surg **17**, 1274–1282 (2013).

[14] Clements, L. W., Chapman, W. C., Dawant, B. M., Galloway, R. L., Miga, M. I., "Robust surface registration using salient anatomical features for image-guided liver surgery: algorithm and validation.," Med. Phys. **35**(6), 2528–2540 (2008).

[15] Rucker, D. C., Wu, Y., Clements, L., Ondrake, J., Pheiffer, T., Simpson, A., Jarnagin, W., Miga, M., "A Mechanics-Based Nonrigid Registration Method for Liver Surgery using Sparse Intraoperative Data.," IEEE Trans. Med. Imaging **33**(1), 147–158 (2014).